©2006 The Visualization Society of Japan and Ohmsha, Ltd.
Journal of Visualization, Vol. 9, No. 4 (2006)381-391

Numerical Flow Visualization of First Cycle and Cyclic Motion of a Rigid Fling-Clapping Wing

Chang, J. W.*[1] and Sohn, M. H.*[2]

*1 Department of Aeronautical Science and Flight Operation, Hankuk Aviation University, 200-1 Hwajeon-dong, Deogyang-gu, Goyang city, Kyeonggi-do, 412-791, Korea.
*2 Department of Aerospace Engineering, Korea Air Force Academy, Ssangsuri, Namil-myun, Chungwon-gun, Chungbuk-do, 363-849, Korea. E-mail: myongsohn@hanmail.net

Received 2 April 2006
Revised 20 June 2006

Abstract : A flow visualization of the two-dimensional rigid fling-clap motions of the flat-plate wing is performed to get the knowledge of fling-clapping mechanism that might be employed by insects during flight. In this numerical visualization, the time-dependent Navier-Stokes equations are solved for two types of wing motion; 'fling followed by clap and pause motion' and 'cyclic fling-clapping motion'. The result is observed regarding the main flow features such as the sequential development of the two families of separation vortex pairs and their movement. For the 'fling followed by clap and pause motion', a strong separation vortex pair of counter-rotation develops in the opening between the wings in the fling phase and they then move out from the opening in the following clap phase. For 'the cyclic fling-clapping motion', the separation vortex pair developed in the outside space in the clap phase move into the opening in the following fling phase. The separation vortex pair in the opening developed in the fling phase of the cyclic motion is observed to be stronger than those of the 'fling followed by clap and pause motion'. Regarding the strong fling separation vortex and the weak clap separation vortex above it in the opening, the flow pattern of the fling phase of the cyclic fling and clap motion is different to that of the fling phase of the first cycle. The flow pattern of the third cycle of the cyclic fling-clapping motion is observed to be almost same as that of the second cycle. Therefore, a periodicity of the flow pattern is established after the second cycle.

Keywords : Fling-clap motion, First cycle, Navier-Stokes equation, Insect flight, Numerical visualization, Separation vortex.

Nomenclature :

c : chord length
C_L : lift coefficient
R_e : Reynolds number
$\vec{r}, \vec{r_0}$: position vector
S_p : power expenditure coefficient
t : time
u, v : velocity component
$\vec{V}, \vec{V_s}$: velocity vector
x, y : coordinates
α : half-opening angle

$\dot{\alpha}$: angular velocity
$\bar{\dot{\alpha}}$: mean angular velocity
Ψ : stream function
ω : vorticity
$\vec{\Omega}$: rotation angular velocity

1. Introduction

Numerous experimental and computational studies (2002 and 2003) been carried out in recent years in order to investigate unsteady aerodynamics associated with insect flight. Dickinson et al. (1999) reported that a comprehensive theory incorporating both translational and rotational mechanisms may explain the diverse patterns of wing motions displayed by different species of insects. Ellington et al. (1996) visualized the airflow around the wings of the hawkmoth *Manduca sexta* and a large 'hovering' mechanical model—the flapper. They found that, during the down-stroke, the leading-edge vortex was of sufficient strength to explain the high-lift forces.

Most of the previous research efforts in this area have focused on the study of cyclic motion in insects. The lift generation mechanism associated with the flight of the small wasp *Encarsia Formosa* was originally formulated by Weis-Fogh (1973), and provides an illustration of the beneficial usage of unsteady flow effects. The fling-clap modes without moving-apart mode occur in nature as discussed in some detail by Maxworthy (1979). Figure 1 illustrates diagrammatically the sequence of fling-clapping wing movements without moving-apart mode. The two wings are identical and are initially close together as shown in Fig. 1(a). The wings open up to form a V shape by rotating around the trailing edge as shown in Figs. 1(b) and (c), which is called the 'fling' phase. After opening up to a certain angle, the leading edges of each wing come together, which is called the 'clap' phase, by rotating around the trailing edge as shown in Figs. 1(d) and (e), and thus the wings return to their initial position shown in Fig. 1(f). After one cycle of wing motion is finished, the two wings repeat the 'fling' phase to start the next cycle.

Maxworthy (1981) reviewed a 'Clap-and-Fling Mechanism' of Weis-Fogh and the 'Butterfly Mechanism'. The wing motion in the fling phase of the 'Butterfly Mechanism' is identical to that in the fling phase of the 'Clap-and-Fling Mechanism'. However, the wing motion in the clap phase is different from that in clap phase of the 'Clap-and-Fling Mechanism'. The wings in the clap phase of the 'Butterfly Mechanism' do not part. However, the trailing edges of butterflies do indeed part as reported by Brodsky (1994). Betts and Wootton (1988) carried out a detailed investigation on butterflies performing various patterns of natural flight. They calculated and compared the kinematic parameters in the representative sequences of four flight modes in which wing shapes were characterized using aspect ratio and non-dimensional moment parameters, and angles described by the extreme limit of wing-stroke from film analysis were in the range of 24° ~ 90° depending on the flight mode and species. Spedding and Maxworthy (1986) measured instantaneous lift by altering the time history of the wing opening and the initial opening angle on

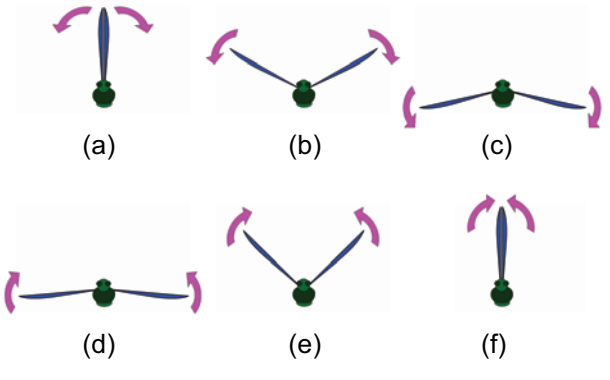

Fig. 1. Fling-clapping wing motion.

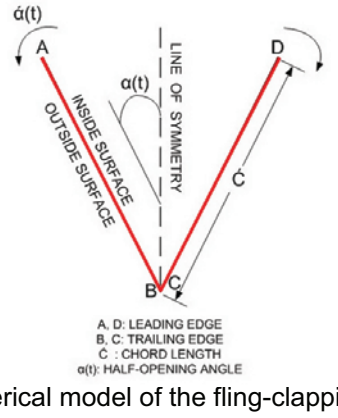

Fig. 2. Numerical model of the fling-clapping wing.

a pair of rigid wings that open as they rotate about a trailing edge. They concluded that the two-dimensional rigid fling is capable of generating high unsteady lift forces associated with high circulations around the separation vortices. Sane (2003) reviewed the basic physical principles underlying flapping flight in insects, the results of recent experiments concerning the aerodynamics of insect flight, and the different approaches used to model these phenomena.

Attention has rarely been given to the investigations of first cycle motion encountered during early stages of flight in insects. Sohn and Chang (2006) reported that the regional circulation for the cyclic fling and clap motion is higher in later cycles than in the first cycle. They concluded that the aerodynamic loads in the fling phase after the second cycle are much greater than those in the fling phase of the first cycle of the wing motion. However, they did not explain the reason why aerodynamic loads of the fling phase are much different in the first cycle and later cycles.

The primary objective of the present study is to provide qualitative data concerning the reason why the aerodynamic loads in the fling phase after the second cycle are much greater than those in the fling phase of the first cycle of the wing motion. Numerical visualizations are performed by using a simple wing model in order to produce two types of two-dimensional rigid fling-clap motions; fling followed by clap and pause, and cyclic fling and clap. The time-dependent Navier-Stokes equations are solved in terms of stream function and vorticity. The wing model of the present numerical study is simple but has essential feature of the fling-clap mechanism.

2. Numerical Procedure

The three-dimensionality of the wing motion and the flexibility of the wing material are of importance in flights of insects and birds in nature. For example, the spanwise flow was found to exist in some insect's flight and play the role of stabilizing and conserving the intense leading vortex as suggested in Van den Berg and Ellington (1997) and Ellington et al. (1996). The analysis of the flexibility wing is needed to obtain the information about the form of flipping, the manner of proper shedding of vorticity and the smooth transition between the several phases of the wing motion cycle in real animal flight. However neglecting these effects is useful in extracting the distinguishing features of the problem. Also the three-dimensionality and the flexibility of the wing is not of great importance in the fling and clap phase of the wing motion cycle as suggested by Weis-Fogh (1973). In the present numerical study, two-dimensional rigid wing of infinitesimal thickness is taken as a wing model both in the fling and clap phase. Straight-line segments AB and CD as shown in Fig. 2 represent the wings. The line segments are joined at the trailing edges B and C, and they perform rotational motion with the axis at the trailing edges. The motions of the two wings are such that they remain mirror images of one another relative to a line of symmetry. The half of the opening angle between the two wings is used as a parameter to describe the wing motion and is designated as α.

In this simulation, only one half of the flow-field, the left half-plane containing the wing AB, is actually solved because of symmetry. The time-dependent Navier-stokes equations in terms of vorticity and stream function are solved by using the integro-differential method, which can confine the solution field to the viscous region only.

The differential governing equations in non-dimensionalized form are as follows.

$$\frac{\partial^2 \Psi}{\partial x^2} + \frac{\partial^2 \Psi}{\partial y^2} = -\omega \tag{1}$$

$$\frac{\partial \omega}{\partial t} + \frac{\partial (u\omega)}{\partial x} + \frac{\partial (v\omega)}{\partial y} = \frac{1}{\mathrm{Re}}\left(\frac{\partial^2 \omega}{\partial x^2} + \frac{\partial^2 \omega}{\partial y^2} \right) \tag{2}$$

In Eqs. (1) and (2) Ψ and ω are stream function and vorticity observed in the stationary reference frame, respectively. The velocity components u and v are x and y components of the velocity vector $\vec{V}$ in the moving reference frame which is attached to the wing AB of Fig. 2. The velocity vector $\vec{V}$ is related to the velocity vector in the stationary reference frame $\vec{V_s}$ by $\vec{V} = \vec{V_s} - \vec{\Omega} \times \vec{r}$ where $\vec{r}$ is the position vector in the moving reference frame, and $\vec{\Omega}$ is the angular velocity of the moving reference frame as seen in the stationary reference frame. The following reference values are used in non-dimensionalization; chord length c for length, mean angular

velocity $\overline{\dot{\alpha}}$ for angular velocity, $1/\overline{\dot{\alpha}}$ for time, $\overline{\dot{\alpha}}$ for vorticity, $\overline{\dot{\alpha}}c$ for velocity, and $\overline{\dot{\alpha}}c^2$ for stream function. Re in Eq. (2) is the flow Reynolds number defined by this equation.

$$\mathrm{Re} = \overline{\dot{\alpha}}c^2 / \nu \tag{3}$$

The integral equations are used to calculate the stream function values of the outer boundary of the computational domain, which is placed at the outer edge of the non-zero vorticity region, and to calculate the surface vorticity values. The integral equation to calculate the stream function values of the outer boundary for wings model of the numerical study (1981) is as follows.

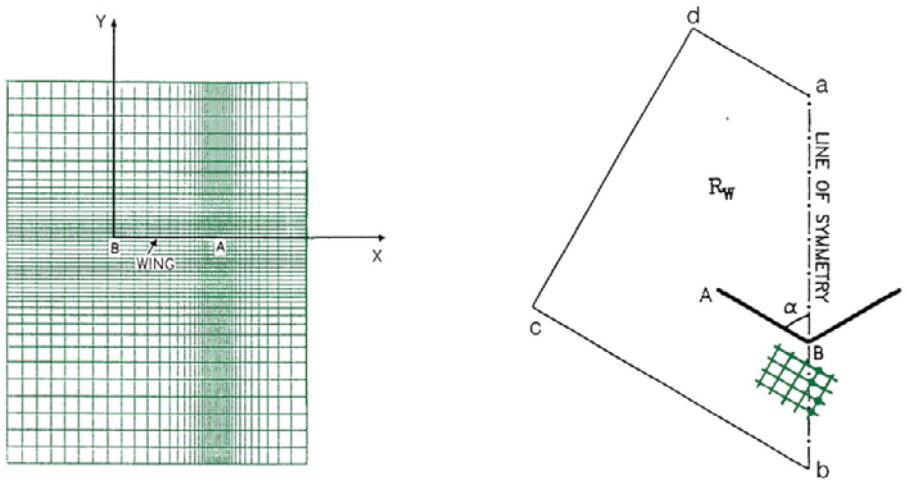

(a) Moving reference frame (b) Computational domain

Fig. 3. Moving reference frame and computational domain.

$$\Psi(\vec{r},t) = \frac{1}{2\pi}\iint_R \omega(\vec{r}_0,t)\ln\frac{|\vec{r}|}{|\vec{r}_0-\vec{r}|}dR_0 \tag{4}$$

In Eq. (4) $\vec{r}$ and $\vec{r}_0$ are position vectors, the integration is performed over the $\vec{r}_0$-space and R is the domain occupied by the fluid. Eq. (4) permits for explicit calculation of the stream function values on the outer boundary point by point by solving Eq. (2). The stream function value on the wing surface is known when the wing motion is prescribed. With stream-function boundary values known, values of stream function in the interior of the solution domain are computed by solving Eq. (1).

A general integral representation for the velocity vector containing boundary integrals as well as a domain integral is presented by Sohn and Wu (1987). For the present problem, the boundary integrals vanish and one has

$$\vec{V}(\vec{r},t) = -\frac{1}{2\pi}\iint_R \omega(\vec{r}_0,t)\times\frac{(\vec{r}_0-\vec{r})}{|\vec{r}_0-\vec{r}|^2}dR_0 \tag{5}$$

2.1 Boundary Conditions and Discretization of the Governing Equations

A non-uniform rectangular grid system is used. This grid is body-fitted to the wing AB shown in Fig. 3(a). Computations are carried out in the left half-plane. The symmetry of the flow-field is utilized to determine the flow in the right half-plane. The outer boundary of the computational domain is composed of four line segments shown schematically in Fig. 3(b). The computational domain expands as the half-opening angle increases. On the line segment *ab* the vorticity and the stream function values are zero because of symmetry. This line, however, is not a grid line. In the present work, vorticity values are taken to be zero at grid points in the immediate vicinity of the line of symmetry. The vorticity values are expected to be negligibly small in the vicinity of the line of symmetry. This expectation has been confirmed by the numerical results obtained in this study. Stream function values at grid points of the outer boundary are calculated using the integral representation of the stream function, Eq. (4). The stream function values on the wing surface boundary are given by the prescribed wing motion.

In discretization of the vorticity transport equation, Eq. (2), first order backward differencing is used for the time derivative and second order central differencing is used for the diffusion term. Upwind differencing is used for the convection term of Eq. (2). Second order central differencing is used for Laplacian operator in Poisson's equation for the stream function shown in Eq. (1). The Successive over-relaxation procedure (SOR) is applied in solving the finite difference equations resulting form the discretization of Eqs. (1) and (2). Detailed numerical procedures are described in Sohn (1986), who developed a numerical method of solving the time-dependent incompressible Navier-Stokes equations in the integro-differential formulation based on Wu (1984). The reliability and accuracy of the numerical method has been ascertained.

2.2 Aerodynamic Load Calculation

For a rotating body of arbitrary shape, one obtains the following reduced equation on the body surface by taking the tangential component of the Navier-Stokes equation of the moving reference attached to the body, and expresses it in terms of the velocity vector and the pressure P.

$$\frac{1}{\rho}\frac{\partial P}{\partial s^*} = \nu\left(\frac{\partial \omega}{\partial n}\right)_B - \dot{\Omega} r^2 \frac{d\theta}{ds^*} + \Omega^2 r \frac{dr}{ds^*} \tag{6}$$

In Eq. (6), Ω is the angular velocity of the body, n is outward normal coordinate, (r(s*), θ(s*)) is the polar coordinates of the body surface with a parameter s* being the tangential coordinate, and the subscript B denoting the body surface condition. For the wing model of the present study, the term $d\theta/ds^*$ in Eq. (6) is zero and the radial coordinate r coincides with the tangential coordinate since the wing is represented by an infinitesimally thin plate and the origin of the moving reference frame is also the origin of the polar coordinates.

Then by integrating Eq. (6) one obtains the following equation for the pressure coefficient Cp defined as $\mathrm{Cp} = 2\,[\mathrm{P(s)} - \mathrm{P\ (\ trailing\ edge\ )}]/\ \rho(\bar{\dot{\alpha}}c)^2$ and S being the non- dimensional tangential coordinate.

$$C_P(S) = \int_0^S \frac{2}{\mathrm{Re}}\left(\frac{\partial \omega}{\partial n}\right)_B d\sigma + \dot{\alpha}^2 S^2 \tag{7}$$

The lift coefficient C_L is defined by

$$C_L = \frac{L}{\frac{1}{2}\rho \overline{\dot{\alpha}^2} c^3} \tag{8}$$

The power expenditure defined by $P_e = \int_0^c (P_{Outside\,surface} - P_{Inside\,surface})\dot{\alpha} S dS$ is the power required for the wing to sustain the rotational motion overcoming the pressure acting on it. The power expenditure coefficient S_p defined as

$$S_p = \frac{P_e}{\frac{1}{2}\rho \overline{\dot{\alpha}^3} c^4} \tag{9}$$

3. Result and Discussions

3.1 First Cycle Motion (Fling → Clap → Pause)

Two types of fling-clap motions are investigated. The first type of wing motion is 'fling followed by clap and pause' to get the knowledge of the first cycle that might be employed by butterflies, which is described as follows.

$$\begin{aligned} &\alpha(t) = 5.428[1-\cos(2\pi t)]/2\pi + 0.0649 \ \text{rad} \\ &\dot{\alpha}(t) = 5.428\sin(2\pi t) \ \text{rad/sec} \quad \text{for} \ 0 \le t \le 1.0 \\ &\alpha(t) = 0.0649 \ \text{rad} \qquad \dot{\alpha}(t) = 0 \ \text{rad/sec} \quad \text{for} \ 1.0 \le t \le 1.5 \end{aligned} \tag{10}$$

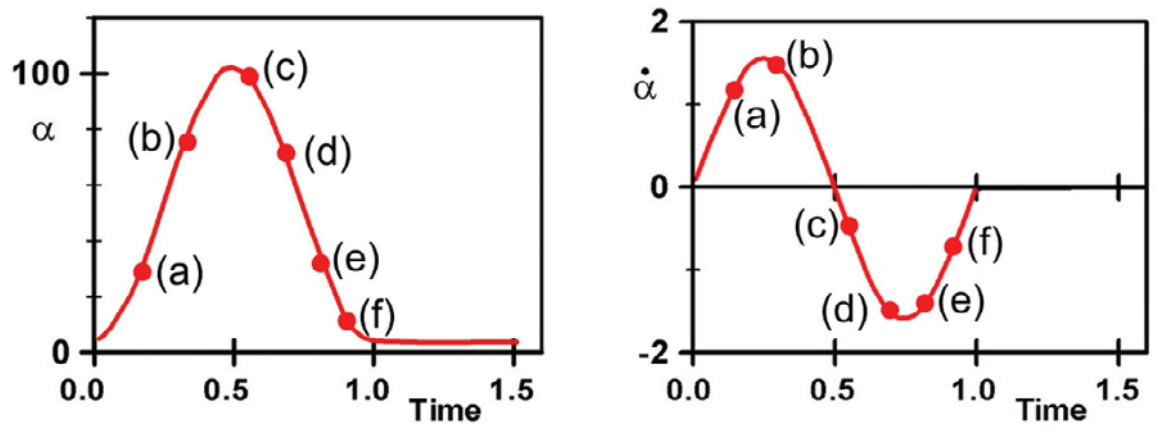

(a) Half-opening angle history (b) Angular velocity

Fig. 4. Description of the first cycle motion.

In this wing motion the wing starts the fling phase with an initial half-opening angle of 3.7° and ends the fling phase at t = 0.5 with a maximum half-opening angle 102.7°. This fling phase is followed by the clap phase, which is the reversed motion of the fling phase. The period of the first cycle motion is 1.0 sec and the mean angular velocity during the fling phase is 3.46 rad/sec. The flow Reynolds number based on this mean angular velocity and the wing chord of the experimental model is about 5,600. The first cycle motion of numerical wing model is shown in Fig. 4. The motion phases corresponding to (a) through (f) of Fig. 5 are marked on the motion history of Fig. 4 for later convenience.

Figure 5 shows the stationary streamlines at various half-opening angles for the first cycle motion. The streamlines of Fig. 5 denote the stream function values between –1.25 and 1.35 with an equi-increment of 0.04. The streamlines of Fig. 5 show that the ambient fluid is pumped into the opening between the wing and the line of symmetry (or between the two wings) in the early moment of the fling phase (Fig. 5(a)). As the fling phase proceeds, the streamlines in the opening detach from the wing surface and form closed lines (Fig. 5(b)). These streamlines develop into flow pattern similar to a solid body rotation with the rotating axis in the interior fluid region. The rotation is clockwise in the left half-plane. Previous investigators used 'leading edge separation vortex' in describing these streamlines because a separation vortex is defined to exist when a relative extreme of vorticity appears in the interior fluid region and it manifests itself in the streamline patterns consisting of either closed or wavy streamlines. In describing the closed streamlines the same expression will be used in this study.

In the clap phase following the fling phase, another separation vortex having opposite sense of rotation to the separation vortex of the fling phase starts to develop in the outside space of the wing as shown in Fig. 5(c). As the clap phase proceeds, the separation vortex of the opening decays rapidly and the separation vortex of the outside space continues to grow and it eventually becomes a dominant feature of the flow as shown in Figs. 5(d), (e). It was observed that the separation vortex of the opening moves out from it during the clap phase corresponding to Figs. 5 (c), (d) and the opening becomes a region of vorticity free except the boundary layer adjacent to the wing surface. The sparse streamlines in the opening of Fig. 5 (d) show that the fluid velocity is very small there. At later moment of the clap phase the ambient fluid is pumped out from the opening and the streamlines in the outside space develop into flow pattern similar to a solid body rotation as shown in Figs. 5 (e), (f). The streamlines at this moment have ridges whose peaks make a curve connecting the center of the separation vortex to the leading edge of the wing. These ridges are feeding paths of concentrated vorticity from the leading edge region to the separation vortex. The center of the solid-body-rotation-like-streamlines locates at the position of 0.2C apart from the trailing edge and 1.2C apart from the line of symmetry at Fig. 5(f). These separation vortices connected to a subsequent fling-clap motion, inherent in insects like butterflies, show very complicated flow phenomena compared to the first cycle motion.

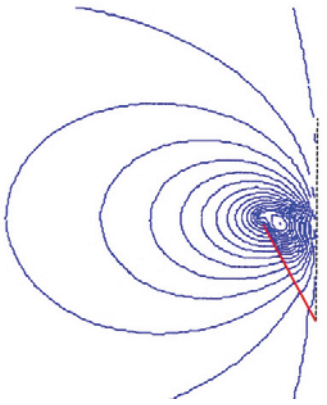

(a) α = 28.3° (fling phase)

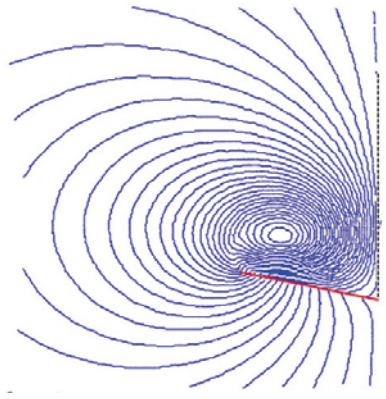

(b) α = 77.2° (fling phase)

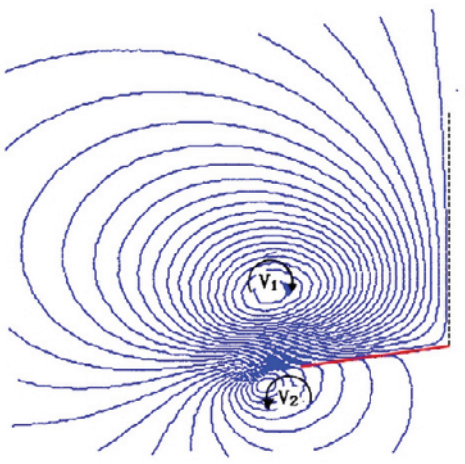

(c) α = 97.2° (clap phase)

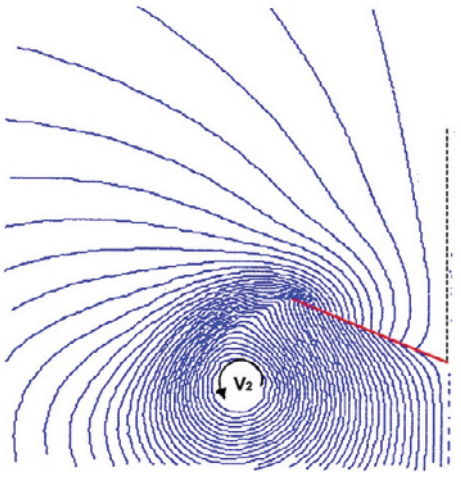

(d) α = 69.0° (clap phase)

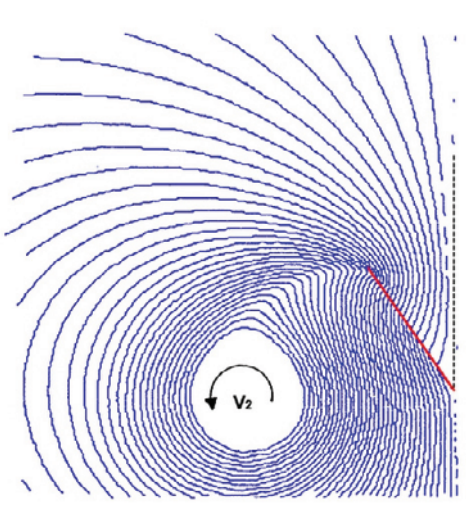

(e) α = 34.8° (clap phase)

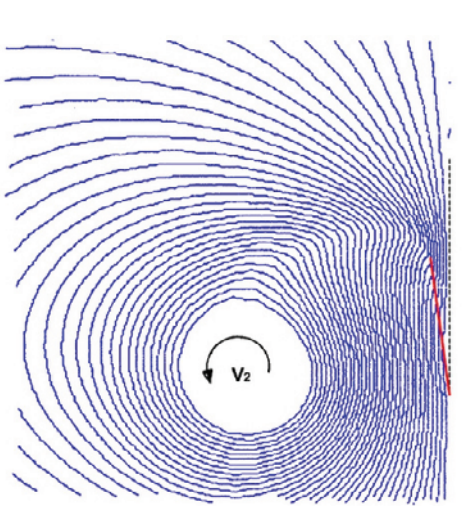

(f) α = 8.3° (clap phase)

Fig. 5. Stationary streamline for the first cycle motion.

3.2 Cyclic Fling-Clapping Motion

The 'cyclic fling-clapping motion' is described as follows.

$$\alpha(t) = 5.428\,[1-\cos(2\pi t)]/2\pi + 0.0649 \quad \text{rad}$$
$$\dot{\alpha}(t) = 5.428\sin(2\pi t) \quad \text{rad/sec} \quad \text{for} \quad 0 \le t \le 3.0 \tag{11}$$

The cyclic fling-clapping motion is solved for investigating the effect of the preceding clap phase to the fling phase or vice versa, and is considered to be more realistic in nature or in experiment. The mean angular velocity and the flow Reynolds number are taken as the same of those of the first type of wing motions. The cyclic fling-clapping motion is shown in Fig. 6.

Sohn and Chang (2006) investigated the time variations of lift and power expenditure coefficients in the cyclic motion of rigid fling- clapping wing. Figure 7 shows the lift and power expenditure coefficient histories from Sohn and Chang (2006). The motion phases corresponding to (a) through (f) of Fig. 8 are marked by open circles on the motion history of Fig. 6 and aerodynamic coefficient histories of Fig. 7 for convenience. The lift and power expenditure histories of Fig. 7 confirm the apparent periodicity after the second cycle of the cyclic fling-clapping motion. Fig. 7 also confirms the fact that a preceding clap phase greatly enhances the aerodynamic loads of the following fling phase while a preceding fling phase does not increase the aerodynamic loads of the following clap phase. In the cyclic fling-clapping motion, the positive lift generated in the fling phase of the second and third cycles is much greater than that of the first cycle. However, the negative lift generated in the clap phase of the second cycle is almost the same as that of the first cycle. The power expenditure of the fling phase of the second and third cycles is much greater than that of the first cycle, and power expenditure of the clap phase of the second cycle is smaller than that of the first cycle.

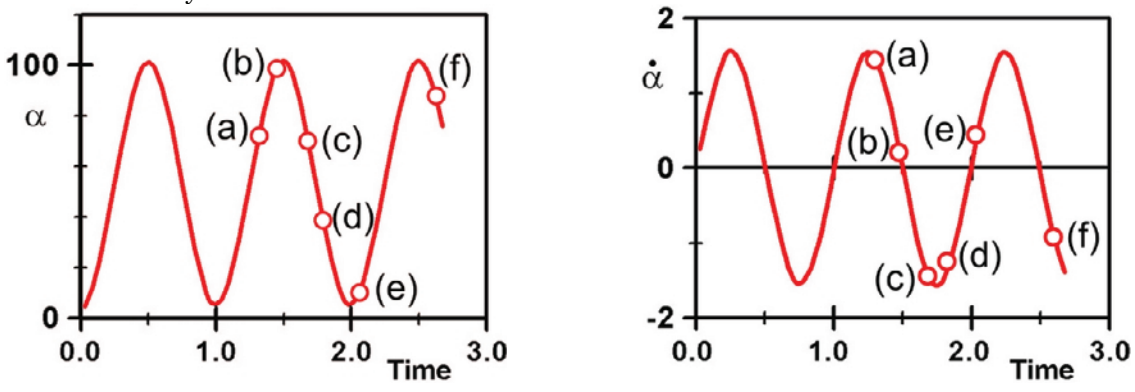

(a) Half-opening angle history (b) Angular velocity

Fig. 6. Description of the cyclic fling-clapping motion.

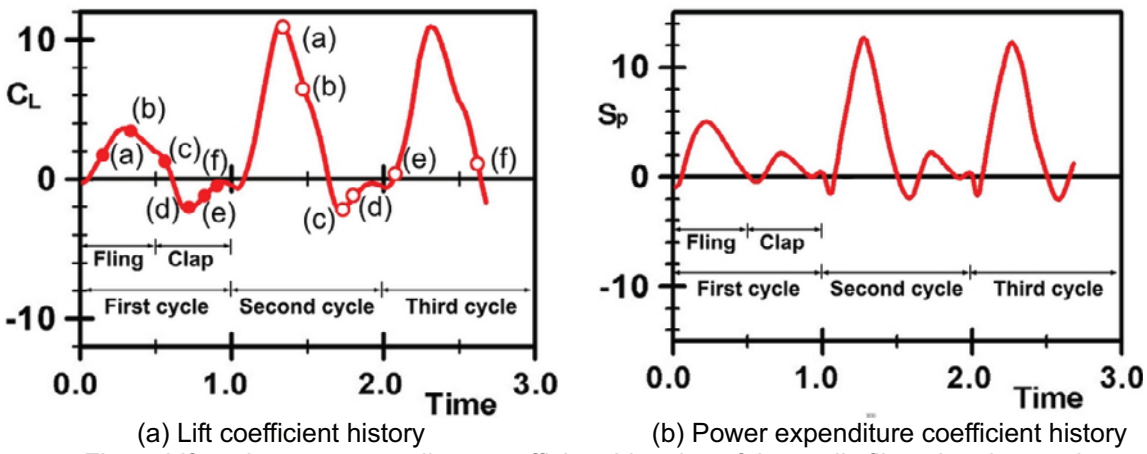

(a) Lift coefficient history (b) Power expenditure coefficient history

Fig. 7. Lift and power expenditure coefficient histories of the cyclic fling-clapping motion (Sohn and Chang, 2006).

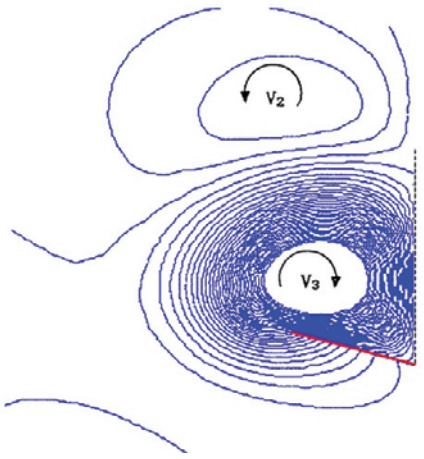

(a) α = 73.9° (fling phase)

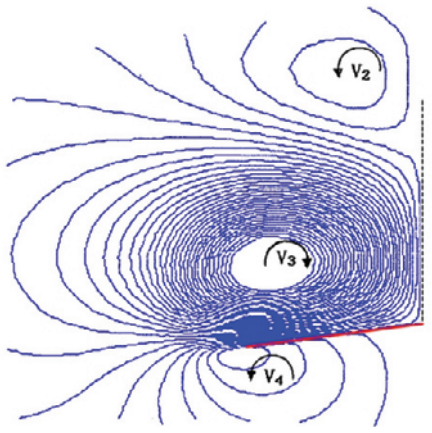

(b) α = 96.9° (clap phase)

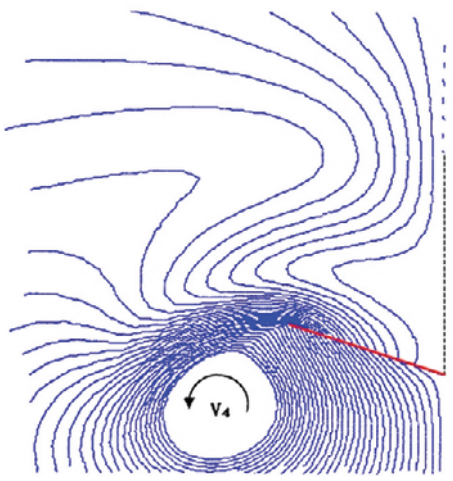

(c) α = 72.1° (clap phase)

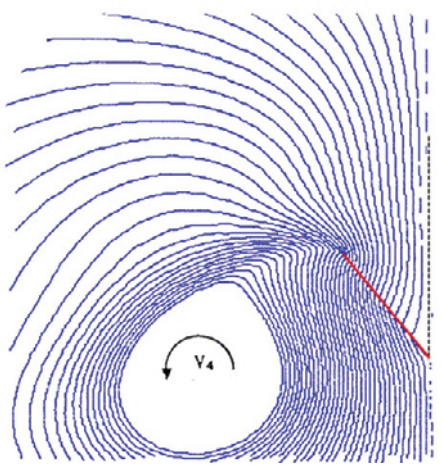

(d) α = 38.8° (clap phase)

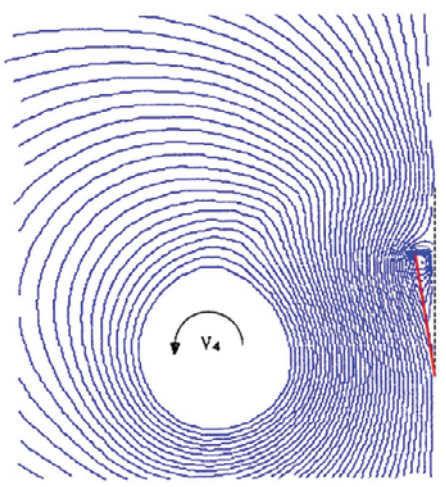

(e) α = 9.0° (fling phase)

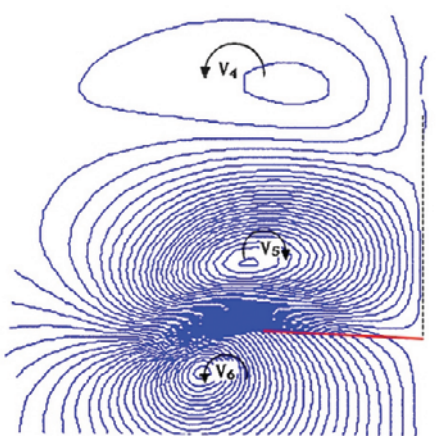

(f) α = 87.5° (clap phase)

Fig. 8. Stationary streamline for the cyclic fling-clapping motion.

Figure 8 shows the flow pattern of the cyclic fling-clapping motion represented by the stationary streamlines, the stream function values of which are in the same range as that of Fig. 5. Since the flow pattern of the cyclic fling-clapping motion is same as that of the first cycle motion for time less than 1.0, the flow pattern of the cyclic fling-clapping motion is shown after t = 1.0 in fig. 8. It is observed that the second-cycle fling vortex V_3 of the cyclic fling-clapping motion in Fig. 8(a) with the first-cycle clap vortex V_2 is much stronger than vortex V_1 of the first cycle motion in Fig. 5 (b). We can say that that the fling vortex of the second cycle and later cycles of the cyclic fling-clapping motion becomes strong due to the existence of the clap vortex of the previous phase in the opening gap, and this causes the larger lift generation after the second cycles.

As the wing begins the second clap phase the counterclockwise separation vortex V_4 develops in the outside space as shown in Fig. 8(b). As the second clap phase proceeds vortex V_4 in the outside space grows and the two separation vortices having different senses of rotation in the opening decay rapidly interacting each other as shown in Fig. 8(c). The two distinct vortices V_2 and V_3 at Fig. 8(b) are no longer identifiable at Fig. 8(c). At later moment of the second clap phase the outside space is dominated by the clap separation vortex V_4 and the opening becomes a region of vorticity free as shown in Fig. 8(d), which is similar to the flow pattern of the clap phase of the first cycle motion in Fig. 5(e). The flow pattern of the third cycle of the fling-clapping motion is observed to be almost same as that of the second cycle. Three distinct vortices are observed in Fig. 8(f), which is the initial clap phase of the third cycle of wing motion. V_4 is the clap vortex of the second cycle, V_5 fling vortex of the third cycle, and V_6 clap vortex of the third cycle. Results show that the flow patterns of the cyclic fling-clapping motion have an apparent periodicity after the second cycle of a fling-clapping wing.

4. Conclusions

A flow visualization of two types of the two-dimensional rigid fling-clap motions; 'fling followed by clap and pause motion' and 'cyclic fling-clapping motion' is numerically performed. In this numerical visualization, the time-dependent Navier-Stokes equations are solved for the wing motion. Main results and conclusions of the present investigation are listed here.

For the 'fling followed by clap and pause motion', a strong separation vortex pair develops in the opening between the two wings in the fling phase. In the clap phase another separation vortex pair having opposite sense of rotation to the separation vortex in the opening develops in the outside space. For 'the cyclic motion', the separation vortex pair developed in the outside space during the clap phase moves into the opening in the following fling phase. It is observed that the separation vortex in the opening developed in the fling phase of the cyclic motion is much stronger than the vortex of the first cycle motion due to the vortex of previous clap motion. Therefore, it can be said that the lift generated during the first cycle of an insect's flight is very different from the lift generated after the second and later cycles.

Regarding the strong fling separation vortex and the weak clap separation vortex above it in the opening, the flow pattern of the fling phase of the cyclic fling-clapping motion is very different to that of the fling phase of the first cycle motion. The flow pattern of the third cycle of the cyclic fling-clapping motion is observed to be almost same as that of the second cycle. Therefore, a periodicity of the flow pattern is established after the second cycle.

References

Betts, C. R. and Wootton, R. J., Wing Shape and Flight Behavior in Butterflies (Lepidoptera: Papilionoidea and Hesperioidea): A Preliminary Analysis, J. Exp. Biol., 138 (1988), 271-288.

Brodsky, A. K., The Evolution of Insect Flight, (1994), 181-186, Oxford University Press.

Dickinson, M. H., Lehmann, Fritz-Olaf, and Sane, S. P., Wing Rotation and the Aerodynamic Basis of Insect Flight, Science, 284 (1999), 1954-1960.

Ellington, C. P., Van den Berg, C., Willmott, A. P. and Thomas, A. L. R., Leading edge Vortices in Insect Flight, Nature, 384 (1996), 626-630.

Maxworthy, T., Experiments on the Weis-Fogh Mechanism of Lift Generation by Insects in Hovering Flight. Part 1. Dynamics of the 'Fling', J. Fluid Mech., 93 (1979), 47-63.

Maxworthy, T., The Fluid Dynamics of Insect Flight, Annual Review of Fluid Mech., 13 (1981), 329-350.

Ramamurti, R. and Sandberg, W. C., A Three-dimensional Computational Study of the Aerodynamic Mechanisms of Insect Flight, J. Exp. Biol., 205 (2002), 1507-1518.

Sane, S. P., The Aerodynamics of Insect Flight, J. Exp. Biol., 206 (2003), 4191-4208.
Sohn, M. H., A Numerical Study of the Weis-Fogh Mechanism, (1986-8), Ph D. Thesis, Georgia Institute of Technology.
Sohn, M. H. and Chang, J. W., Flow Visualization and Aerodynamic Load Calculation of Three Types of Clap-Fling Motions in Weis-Fogh Mechanism, J. Aerospace Science and Technology, (2006), Accepted for publication.
Sohn, M. H. and Wu, J. C., A Numerical Study of the Weis-Fogh Mechanism, AIAA Paper 87-0238, (1987).
Spedding, G. R. and Maxworthy, T., The Generation of Circulation and Lift in a Rigid Two-dimensional Fling, J Fluid Mech., 165 (1986), 247-272.
Van den Berg, C. and Ellington, C. P., The Three-dimensional Leading-edge Vortex of a Hovering Model Hawkmoth: Philosphical Transactions of the Royal Society of London, Series B, 352 (1997), 329-340.
Weis-Fogh, T., Quick Estimates of Flight Fitness in Hovering Animals Including Novel Mechanisms for Lift Production, J. Exp. Biol., 59 (1973), 169-230.
Wu, J. C., Fundamental Solutions and Numerical Methods for Flow Problems, International J. for Numerical methods in Fluids, 4 (1984), 185-201.

Author Profile

Jo Won Chang: He received the B.S. degree in aerospace engineering from Korea Air Force Academy in 1982, and the M.S. and Ph.D. degrees from Seoul National University and KAIST in 1986 and 1999, respectively. He is currently an associate professor in the department of aeronautical science and flight operation at the Hankuk Aviation University in Korea. His research interests include unsteady aerodynamics, bio-fluid mechanics, wind tunnel experiments, and flight tests.

Myong Hwan Sohn: He received the B.S. degree in aerospace engineering from Korea Air Force Academy in 1977, and the M.S. and Ph.D. degrees from Seoul National Univ. and Georgia Institute Technology in 1981 and 1986, respectively. He is currently a professor in the department of aerospace engineering at the Korea Air Force Academy. His research interests include unsteady aerodynamics, bio-fluid mechanics, and computational fluid dynamics.